Supplement of Clim. Past, 19, 959–978, 2023
https://doi.org/10.5194/cp-19-959-2023-supplement


Climate of the Past
Open Access

*Supplement of*

# The effect of uncertainties in natural forcing records on simulated temperature during the last millennium

**Lucie J. Lücke et al.**

*Correspondence to:* Lucie J. Lücke (lucie.luecke@ed.ac.uk)

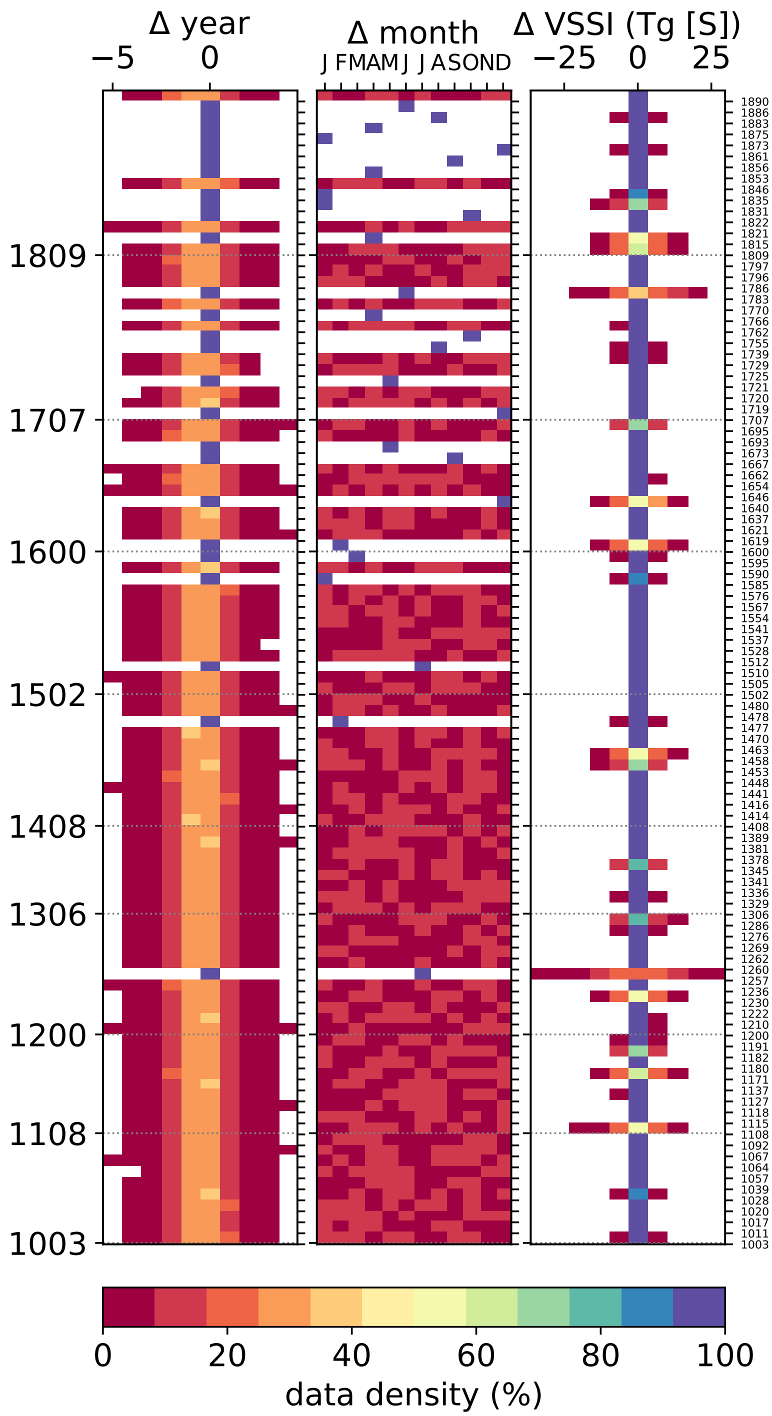

**Figure S1.** Overview of the volcanic forcing ensemble. Left: year of eruption relative to eVolv2k eruption year (eVolv2k eruption year shown on axis label of right panel). Middle: eruption month. Right: volcanic stratospheric sulfate injection (VSSI) relative to eVolv2k. Colour represents the data density. Blue single dots in left and middle panel are dated eruptions. Note that the time axis is not evenly spaced in time but by eruption years (see labels on right panel).

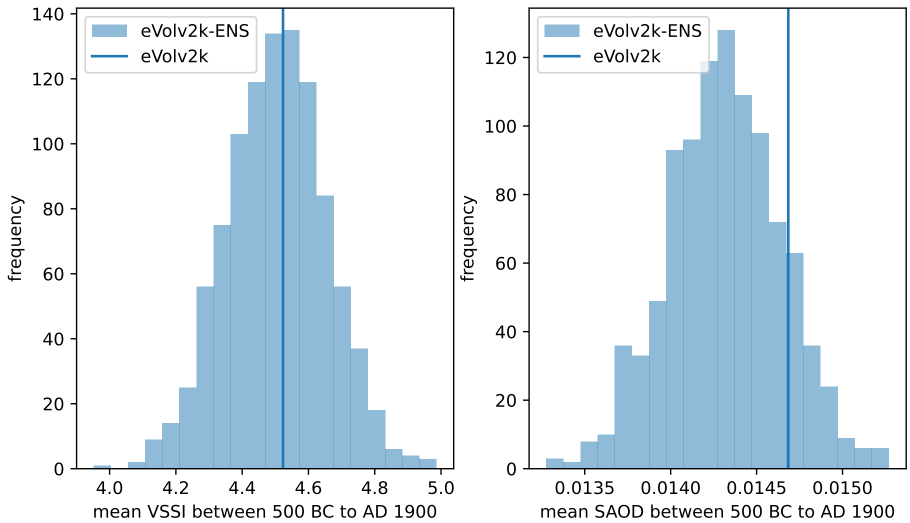


**Figure S2.** Left: mean VSSI of all eruptions between 500 BC and AD 1900 for eVolv2k and the distribution across eVolv2k-ENS. Right: as left panel but for mean SAOD.

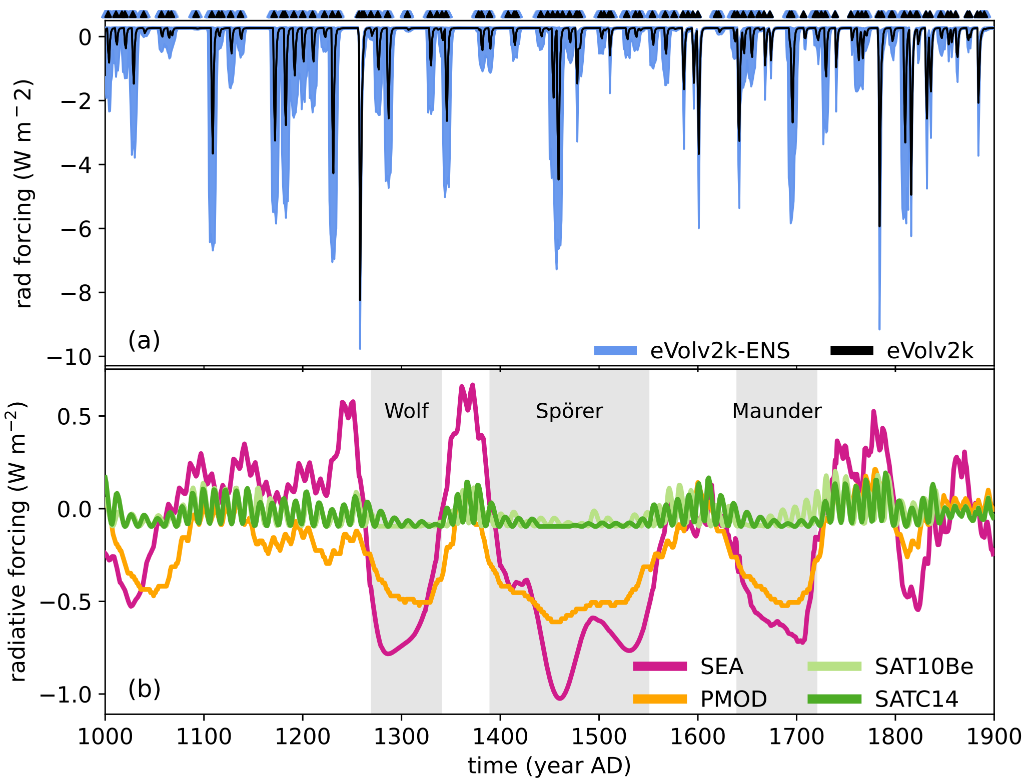


**Figure S3.** As Fig. 1 but with (a) showing NH radiative forcing.

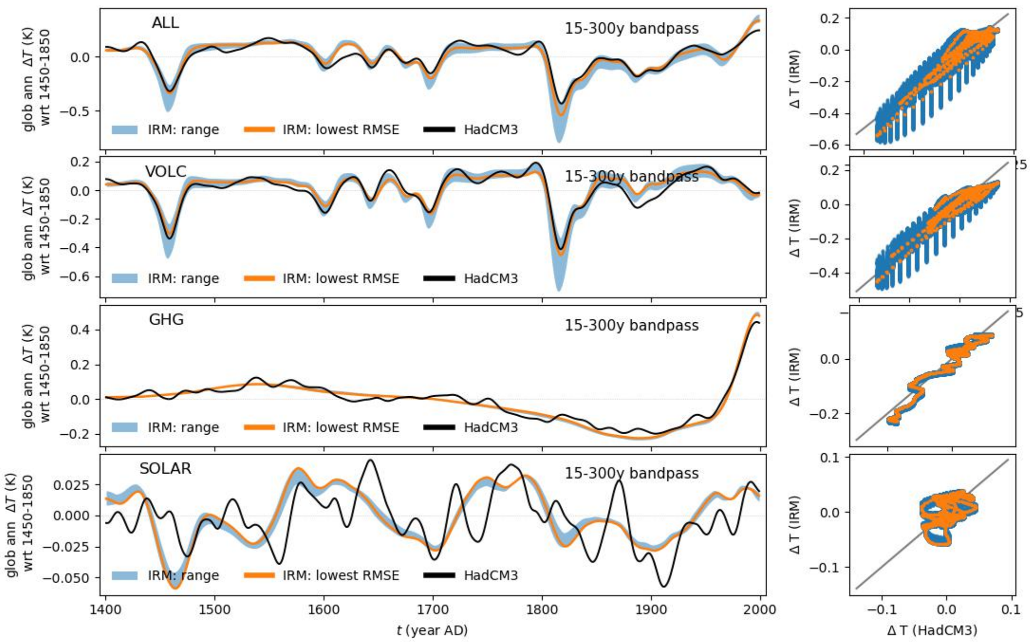


**Figure S4.** HadCM3 ensemble mean versus the response model output and the best fit during the tuning process. Left: Timeseries of the model runs, using (from top to bottom): all forcings, volcanic forcing only, greenhouse gas forcing only, solar forcing only. Right: scatter plot of the timeseries as shown on the left panel: HadCM3 ensemble mean versus each response model run. Colours as stated in legend on left panels.

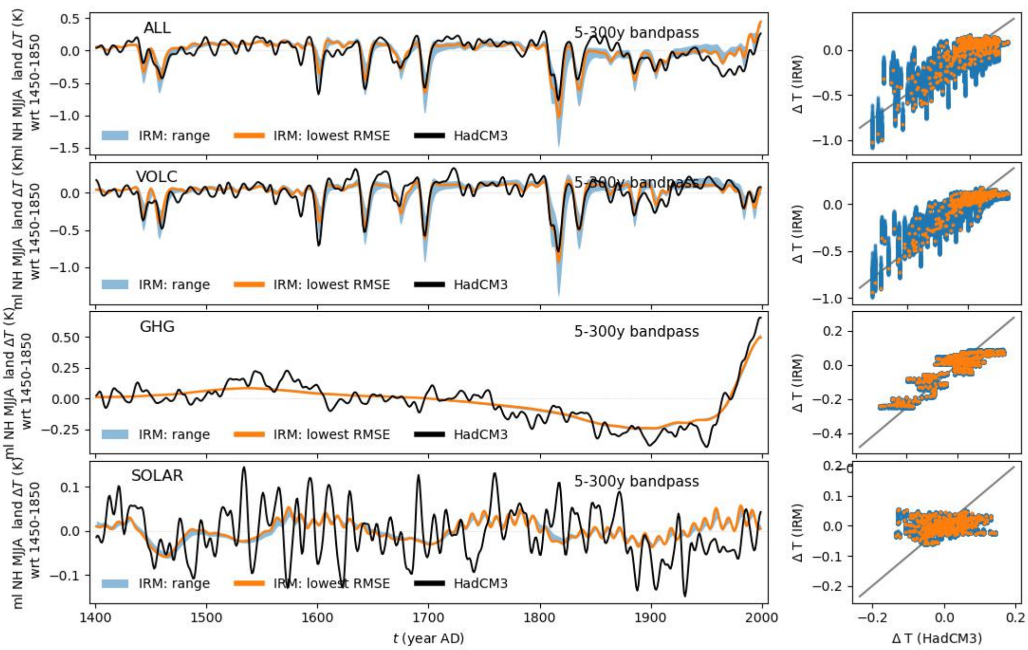


**Figure S5.** As previous but for tuning to midlatitudinal NH summer (MJJA).

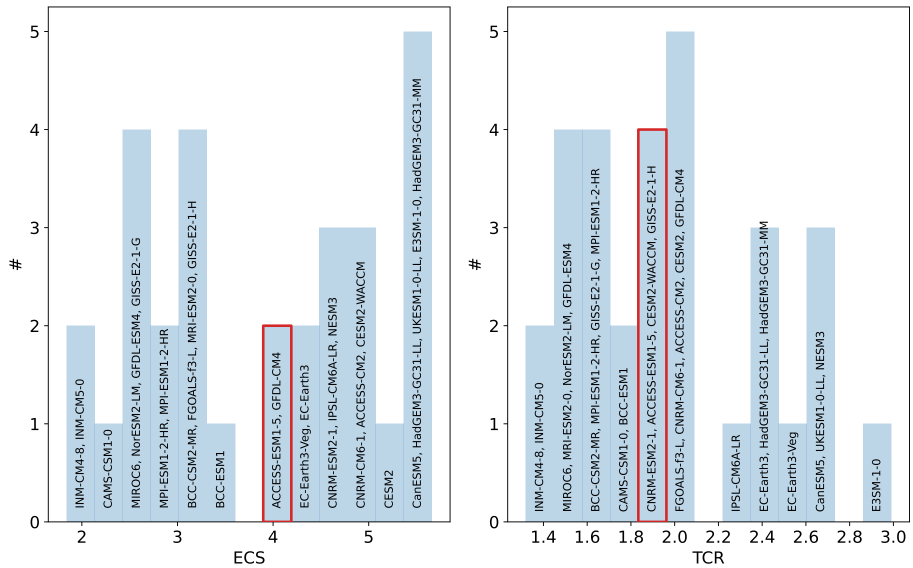


**Figure S6.** ECS and TCR values of the 30 CMIP6 models (Nijsse et al., 2020). Red shading indicates the median value.

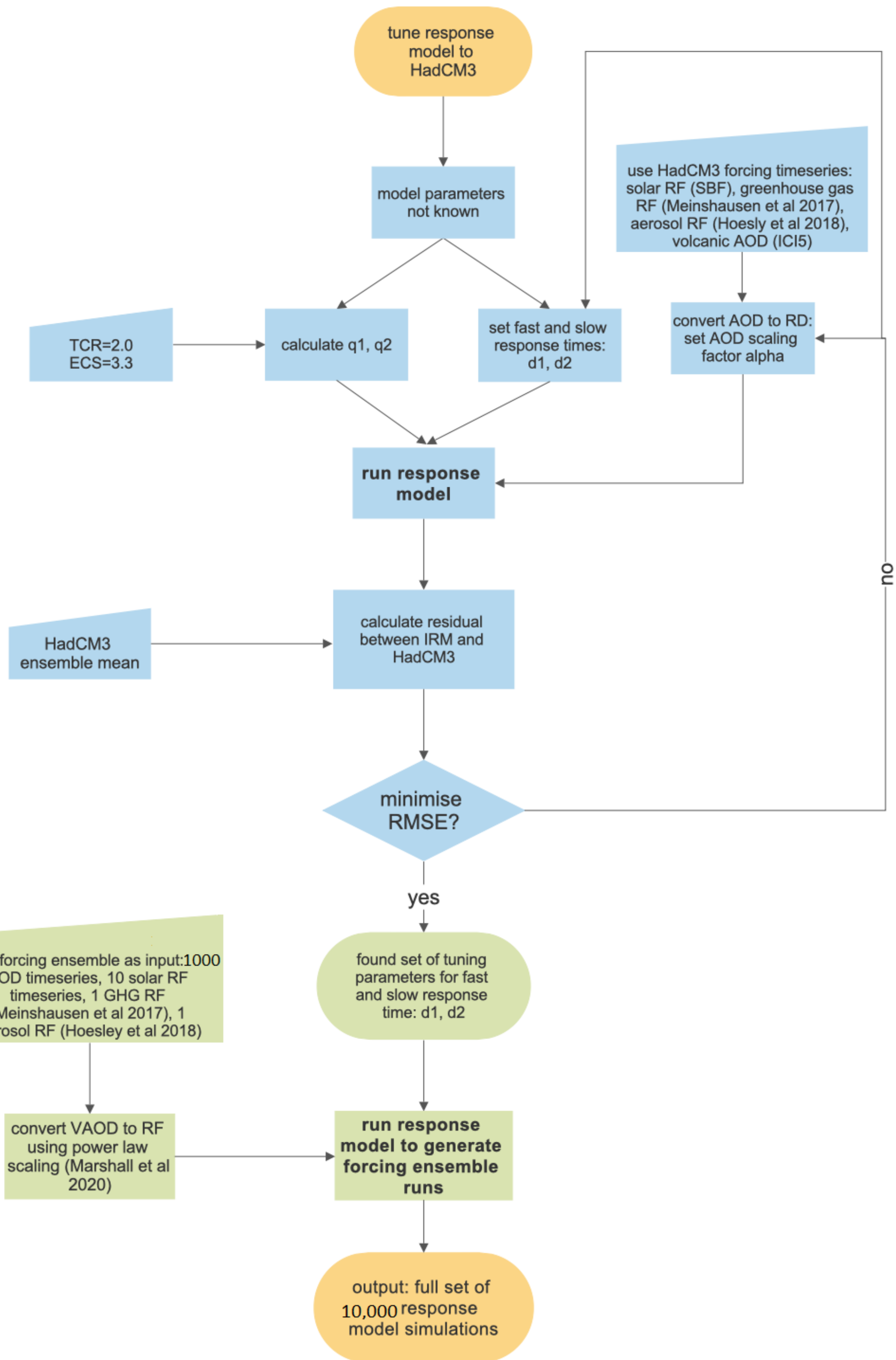


**Figure S7.** Flowchart of the tuning process (blue) followed by the generation of the forcing uncertainty ensemble simulations (green).

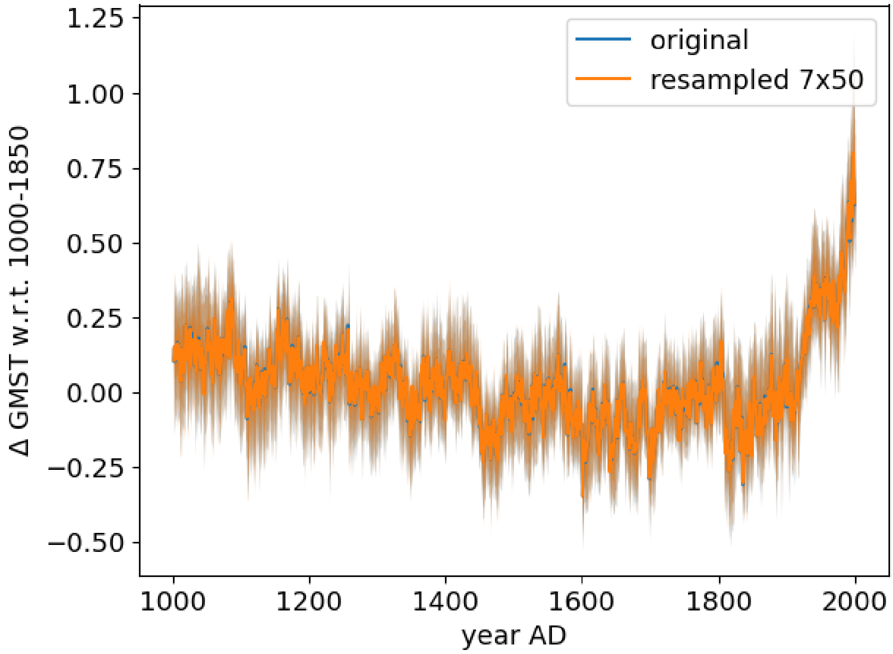


**Figure S8.** Subsampling of 7x50 members of the PAGES2k ensemble versus the full ensemble (7x1000 members)

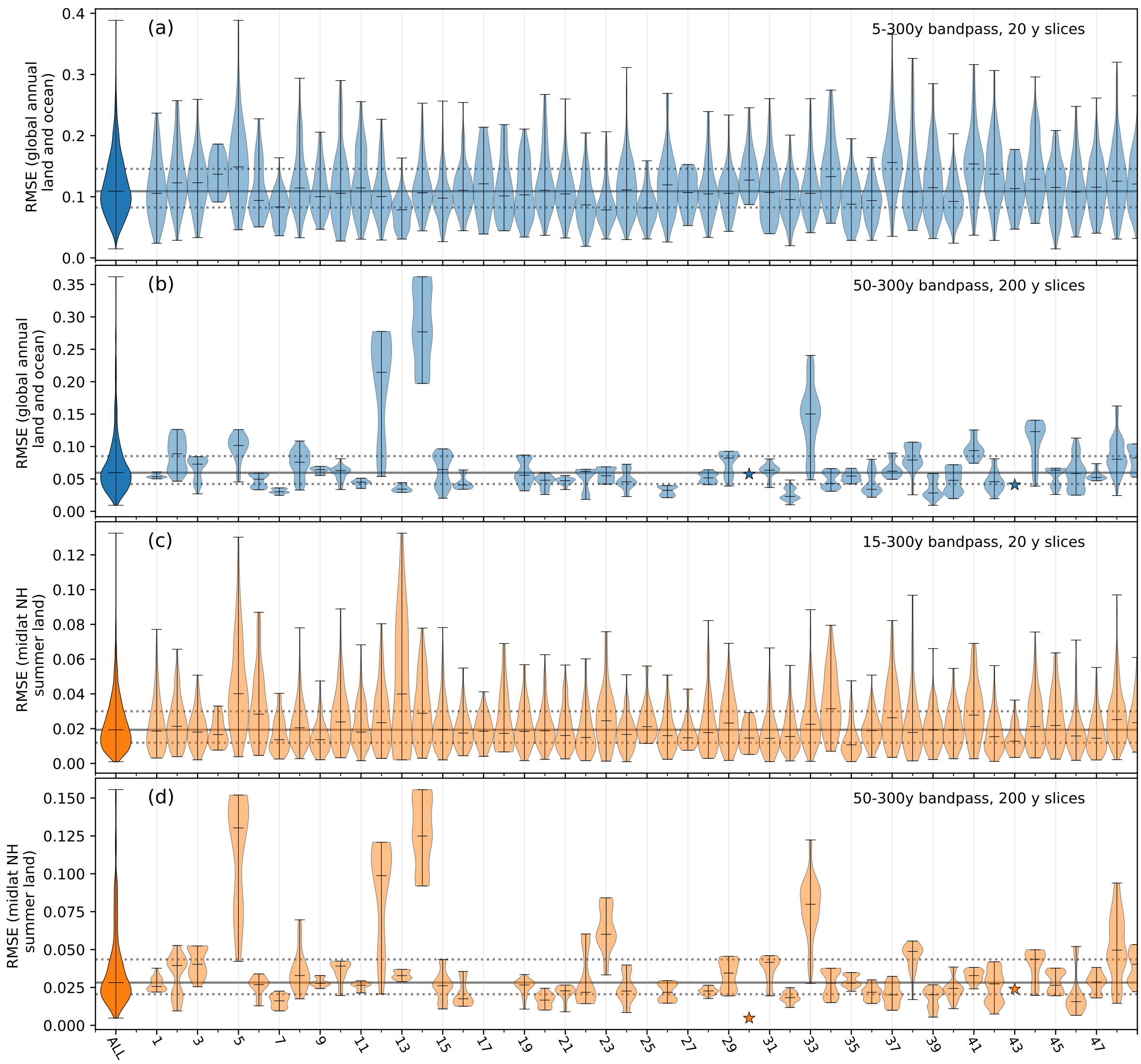


**Figure S9.** Variability of the individual CMIP6 control runs aggregated by model (see table S1 to identify the model names), and the whole CMIP6 population (ALL). (a), (b) non-overlapping 20 year slices (a) and 200 year slices (b) of midlatitudinal NH summer land temperature. (c) and (d) as (a) and (b) but for global annual data. The dashed horizontal line indicates the upper and lower quartile of the whole population. High variability models identified in (c) and (d) coincide with the ones identified by Parsons et al. (2020).

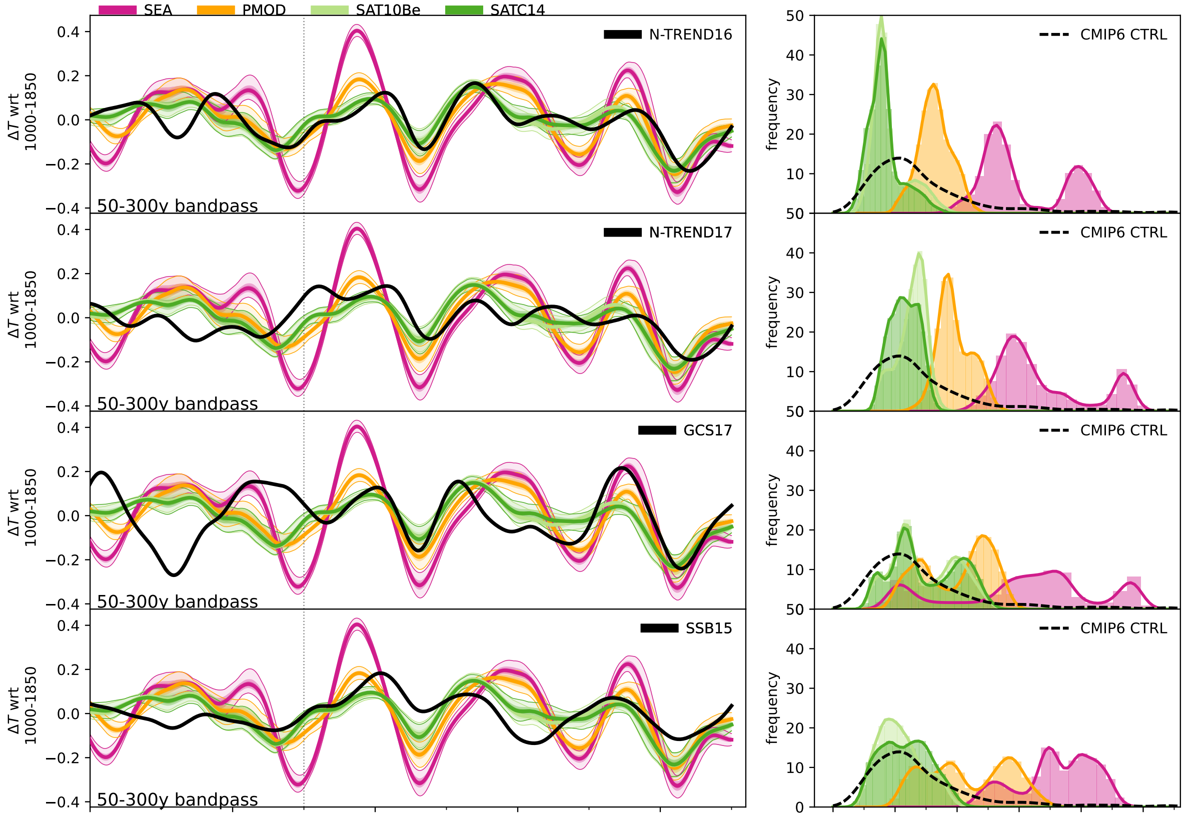


**Figure S10.** As Fig. 3 but for the single NH reconstructions. Top to bottom: N-TREND16 (Wilson et al., 2016), N-TREND17 (Anchukaitis et al., 2017), GCS17 (Guillet et al., 2017) and SSB15 (Schneider et al., 2015).

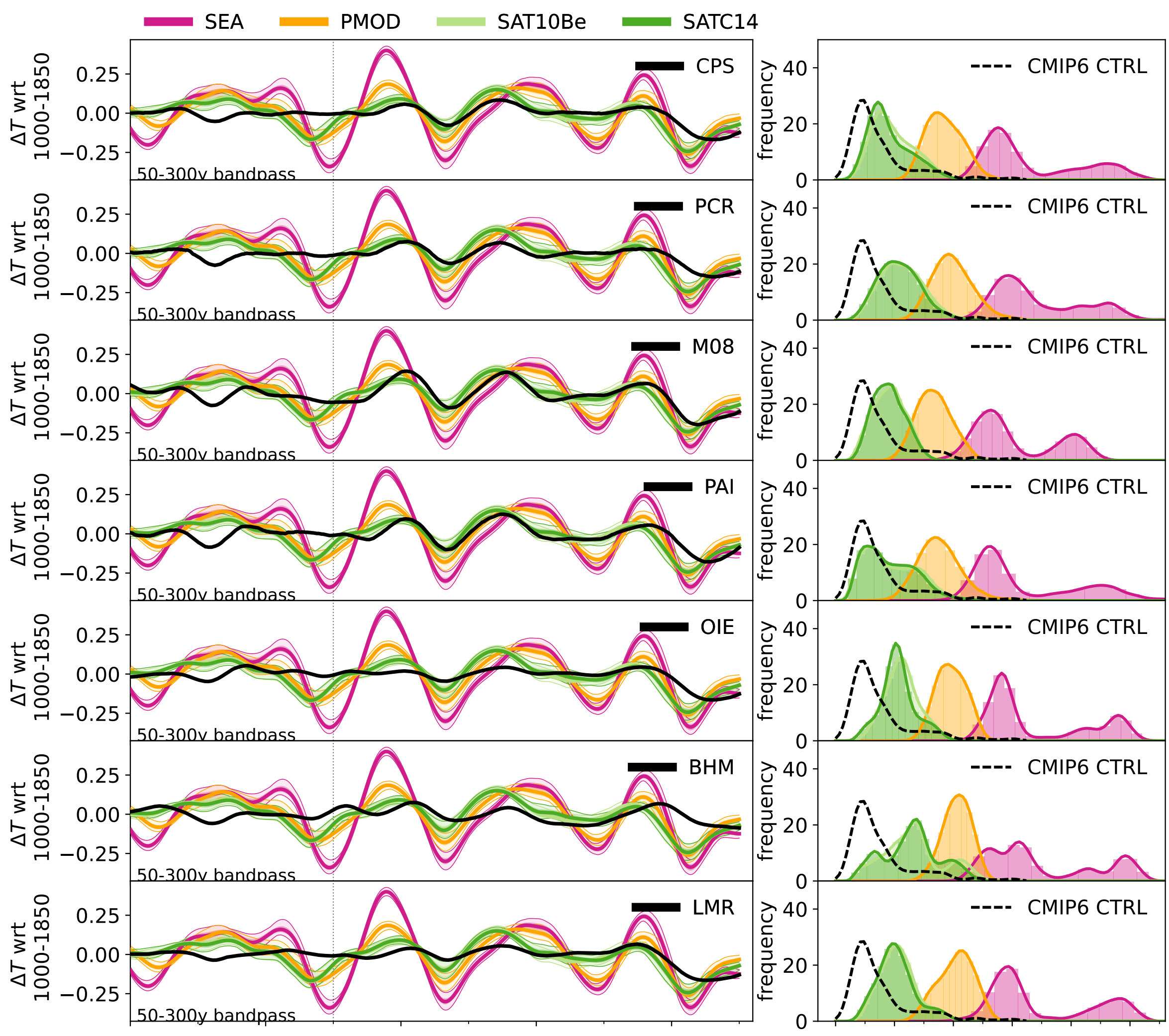


**Figure S11.** As Fig. 3 but for the single PAGES 2k median reconstructions.

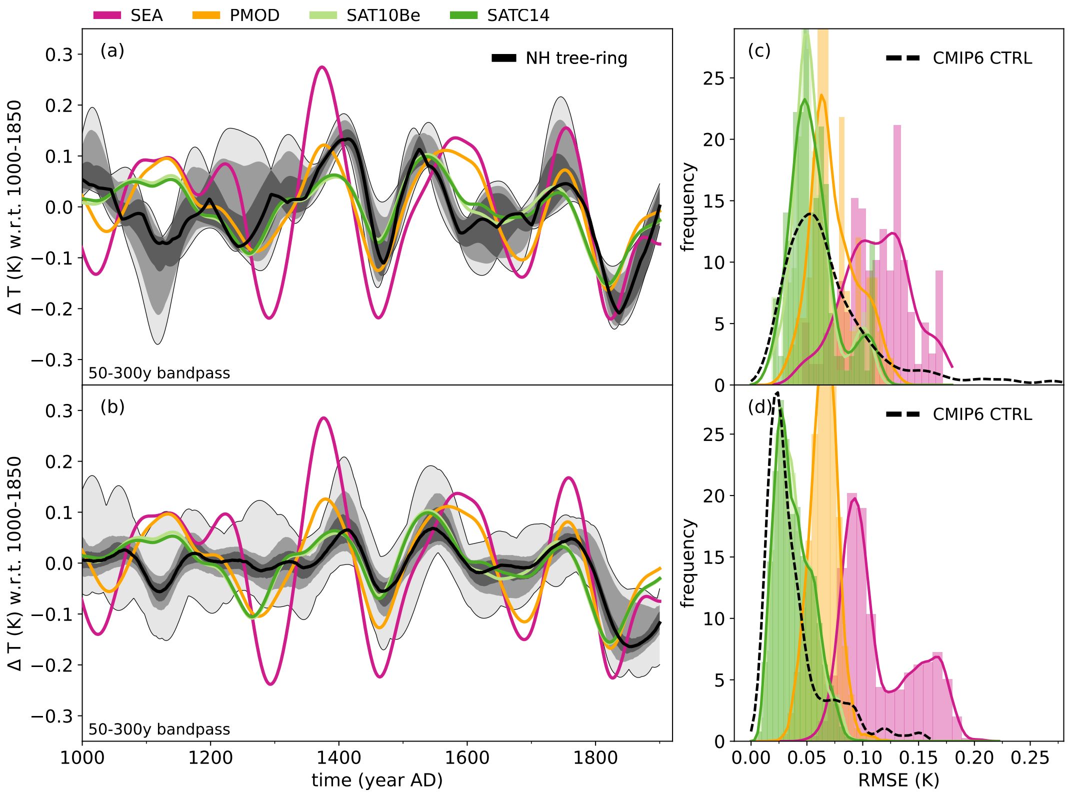


**Figure S12.** As Fig.3 but for low climate sensitivity (ECS=1.84, TCR=1.32 as in INM-CM4-8).

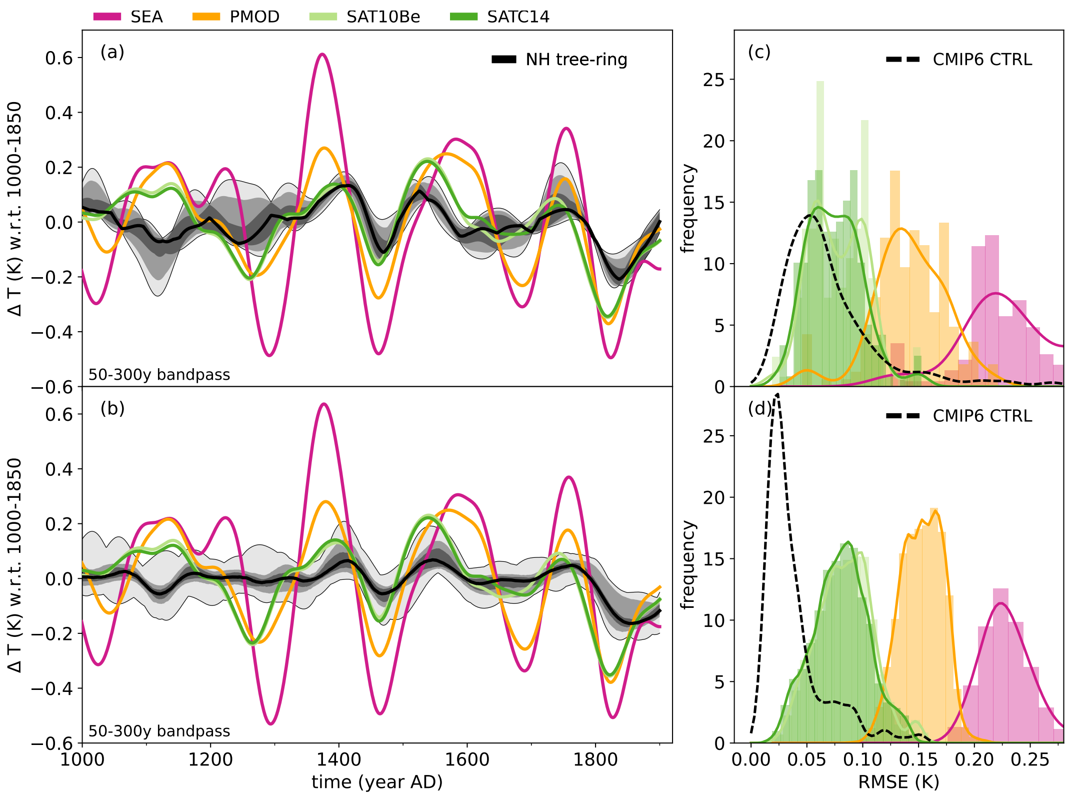


**Figure S13.** As Fig. 3 but for high climate sensitivity (ECS=5.38, TCR=2.99 as in E3SM-1-0).

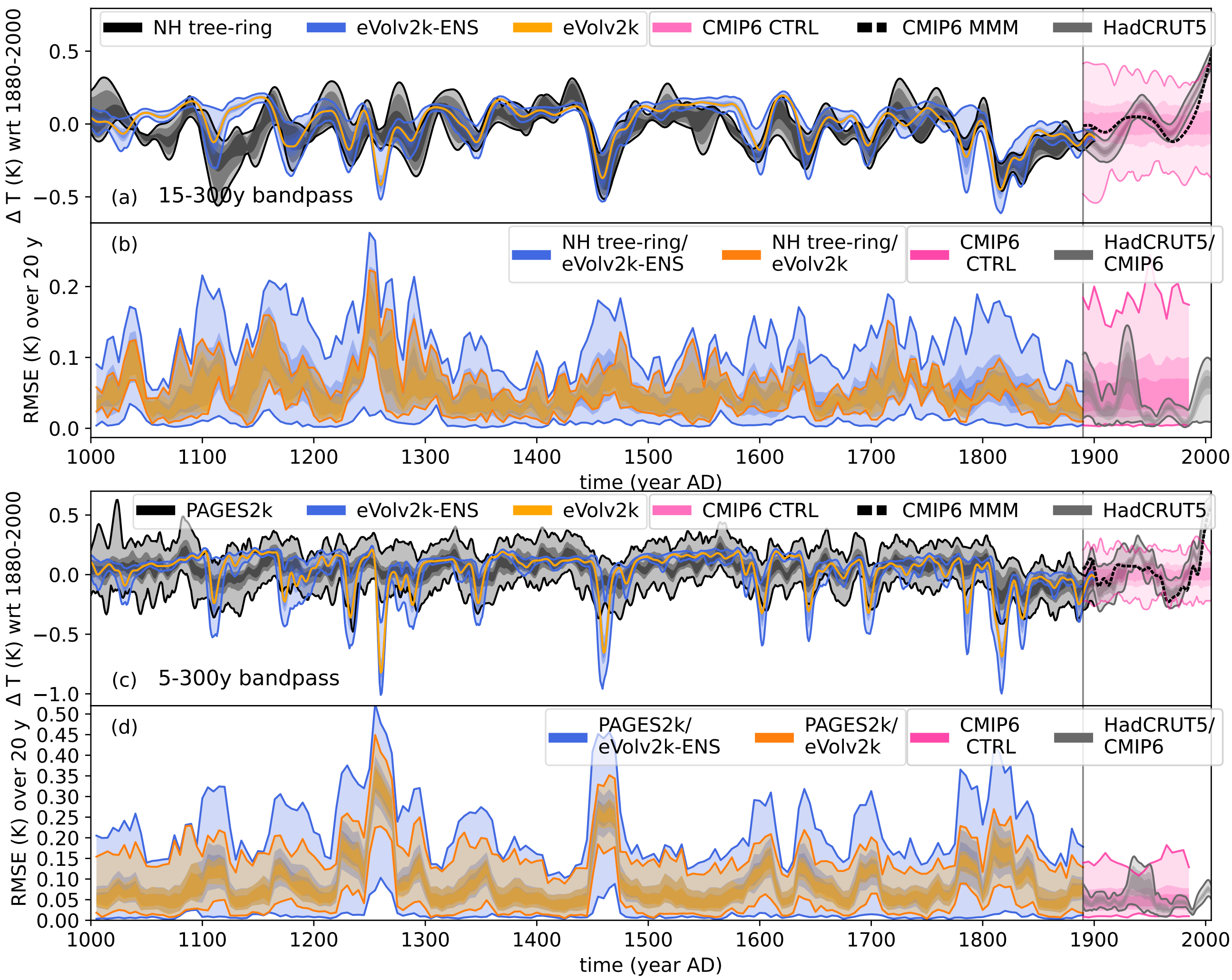


**Figure S14.** As Fig. 4 but with inverted bandpass filters for NH reconstructions and PAGES 2k.

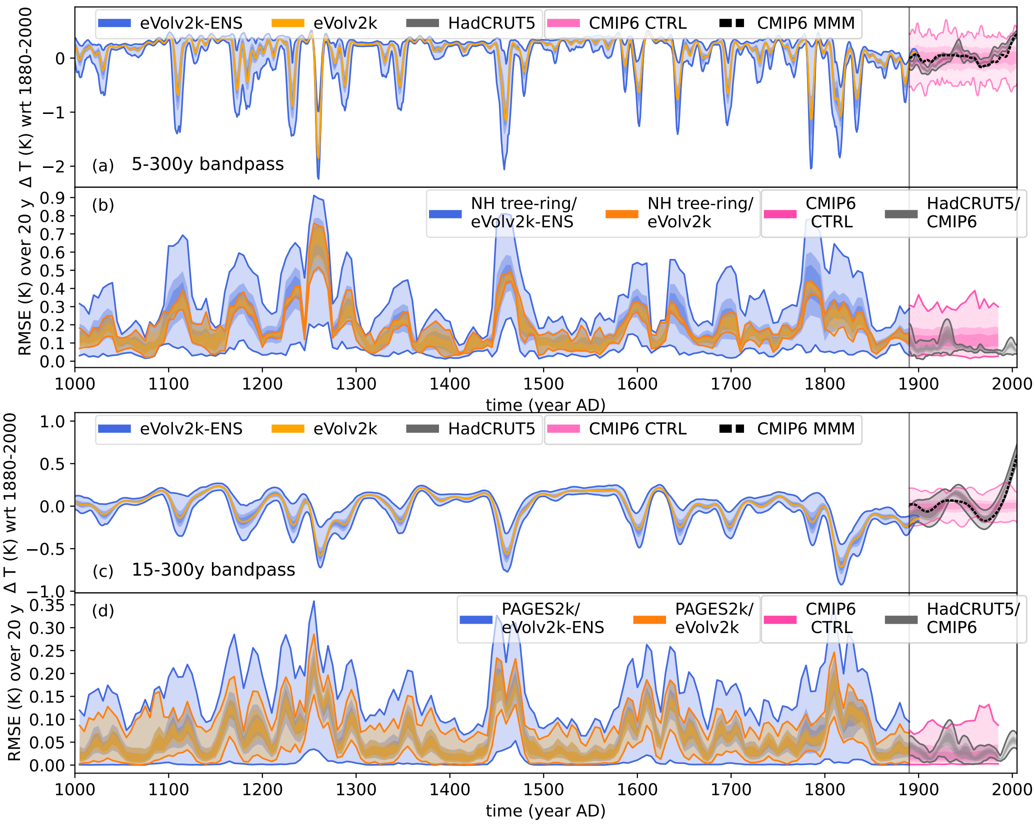


**Figure S15.** As Fig. 4 but for high climate sensitivity (ECS=5.38, TCR=2.99 as in E3SM-1-0).

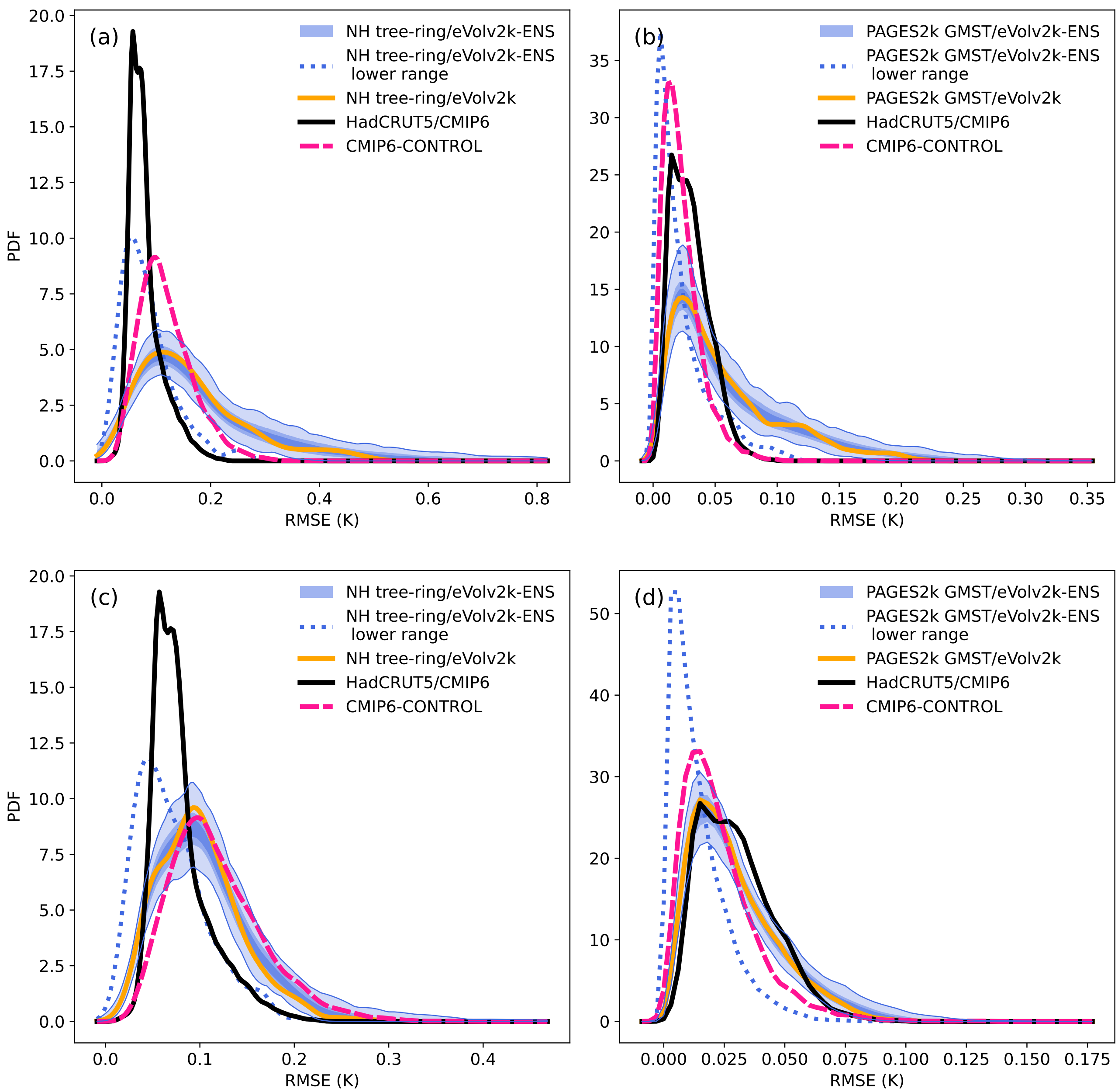


**Figure S16.** As Fig. 5 but for (a), (b) high climate sensitivity (ECS=5.38, TCR=2.99 as in E3SM-1-0) and for (c), (d) low climate sensitivity (bottom, ECS=1.84, TCR=1.32 as in INM-CM4-8).

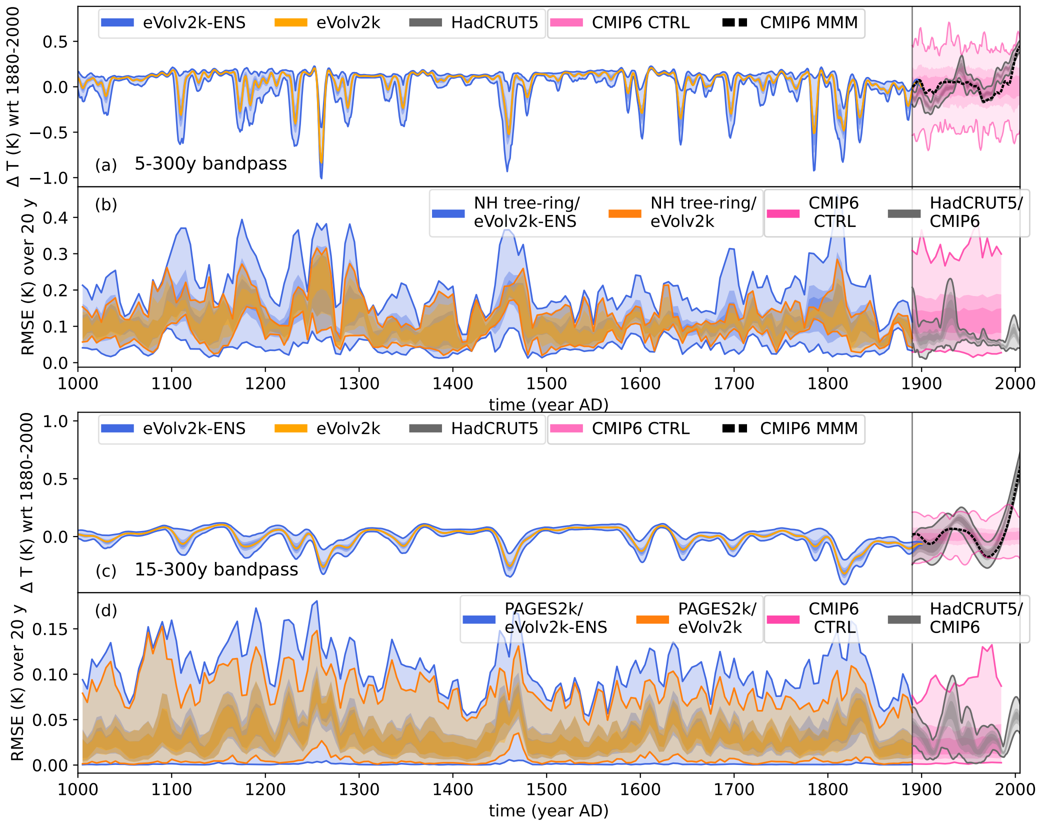


**Figure S17.** As Fig. 4 but for low climate sensitivity (ECS=1.84, TCR=1.32 as in INM-CM4-8).

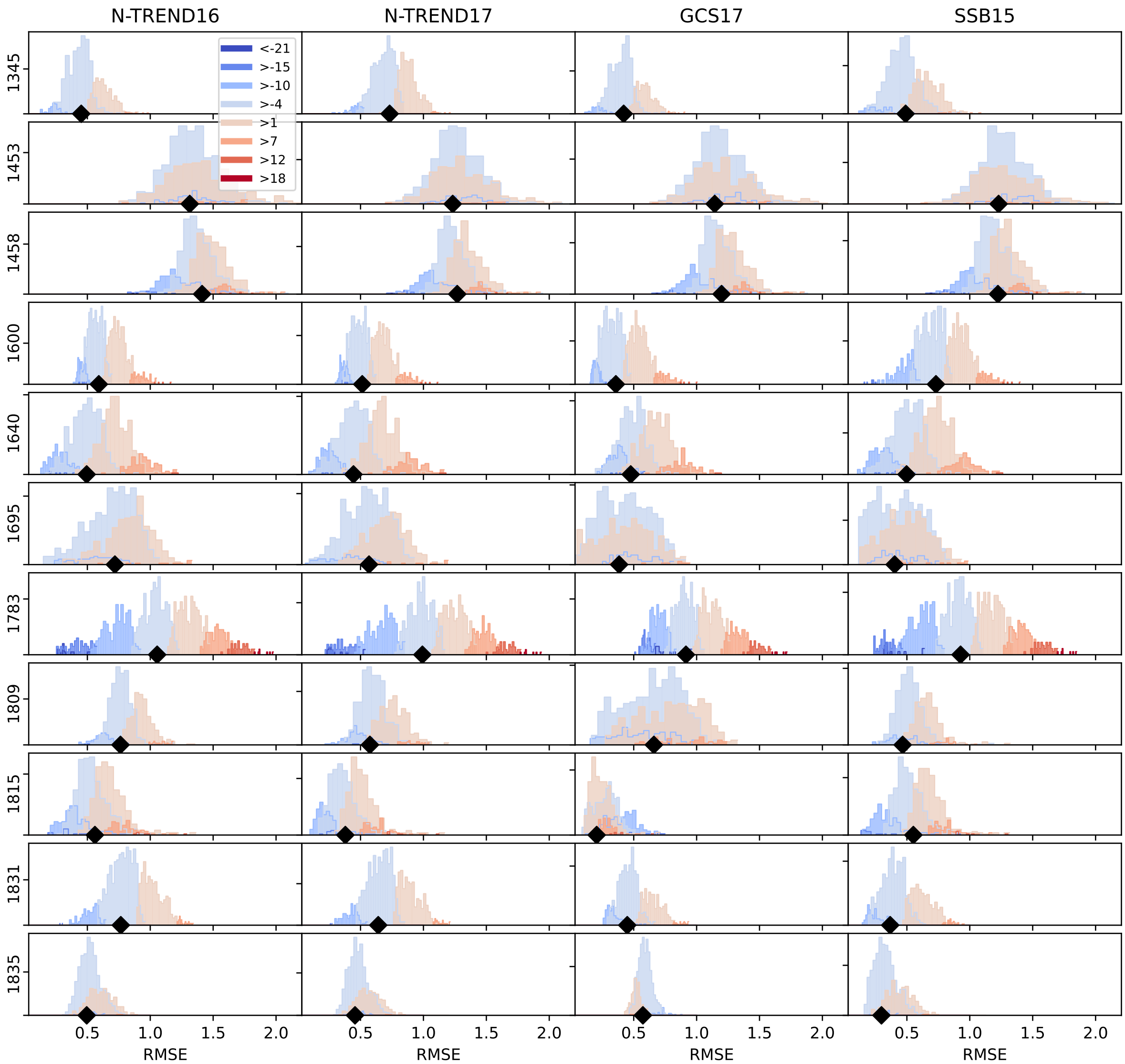


**Figure S18.** Distribution of average residual between NH reconstructions and each member of eVolv2k-ENS, starting in eruption year to 15 years after. In all panels, the data is colour coded depending on the eruption difference in VSSI compared to eVolv2k (see legend in first panel). Black diamond on x-axis shows the RMSE associated with eVolv2k.

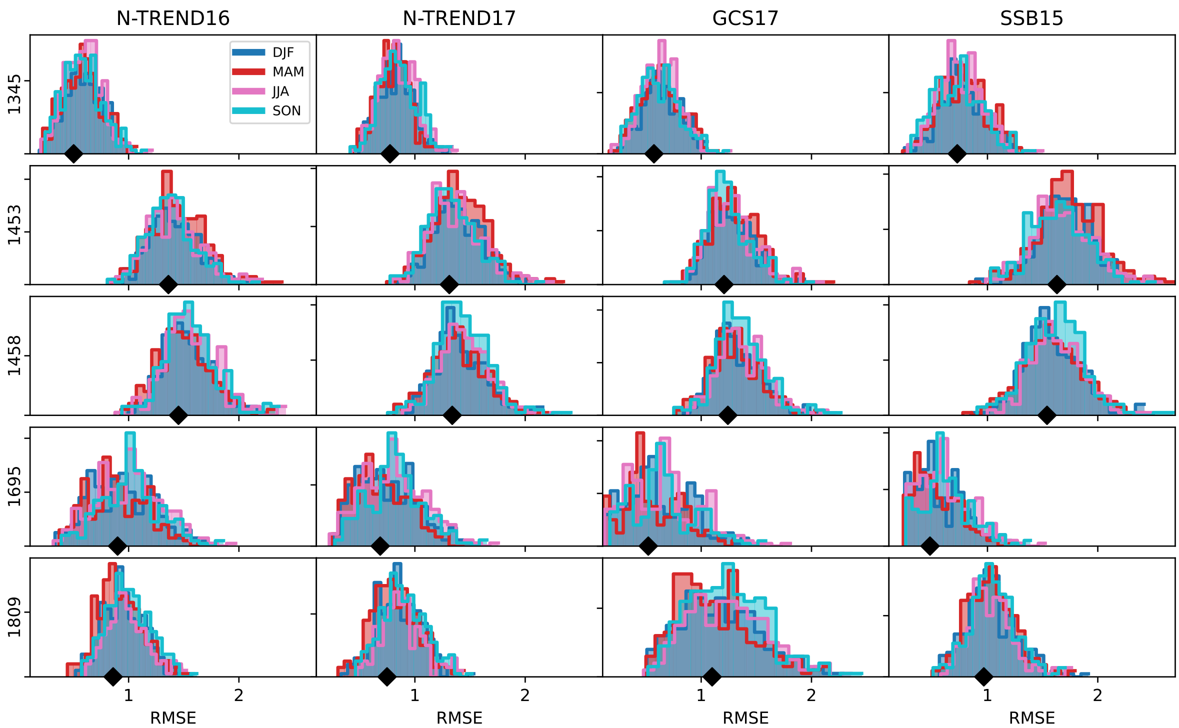


**Figure S19.** As Fig. S18, but showing the eruption season. In eVolv2k all eruptions are assigned to happen in January.

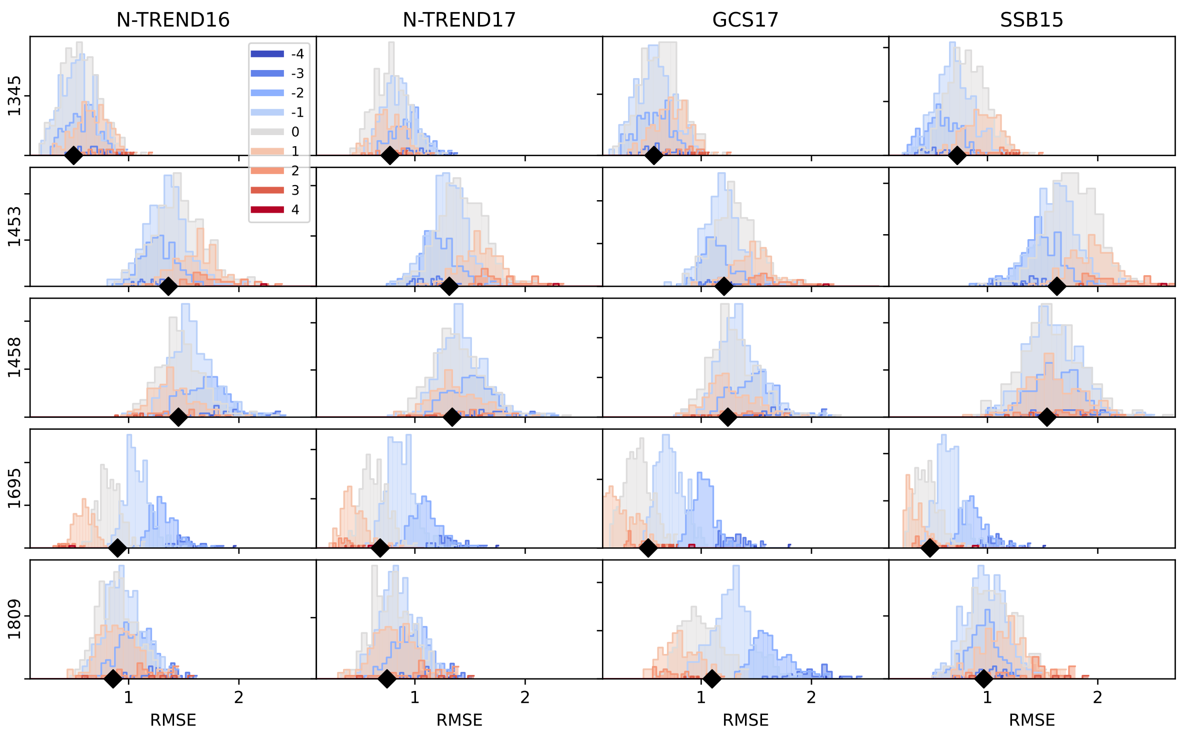


**Figure S20.** As Fig. S18, but showing the difference in eruption year for the undated eruptions only.

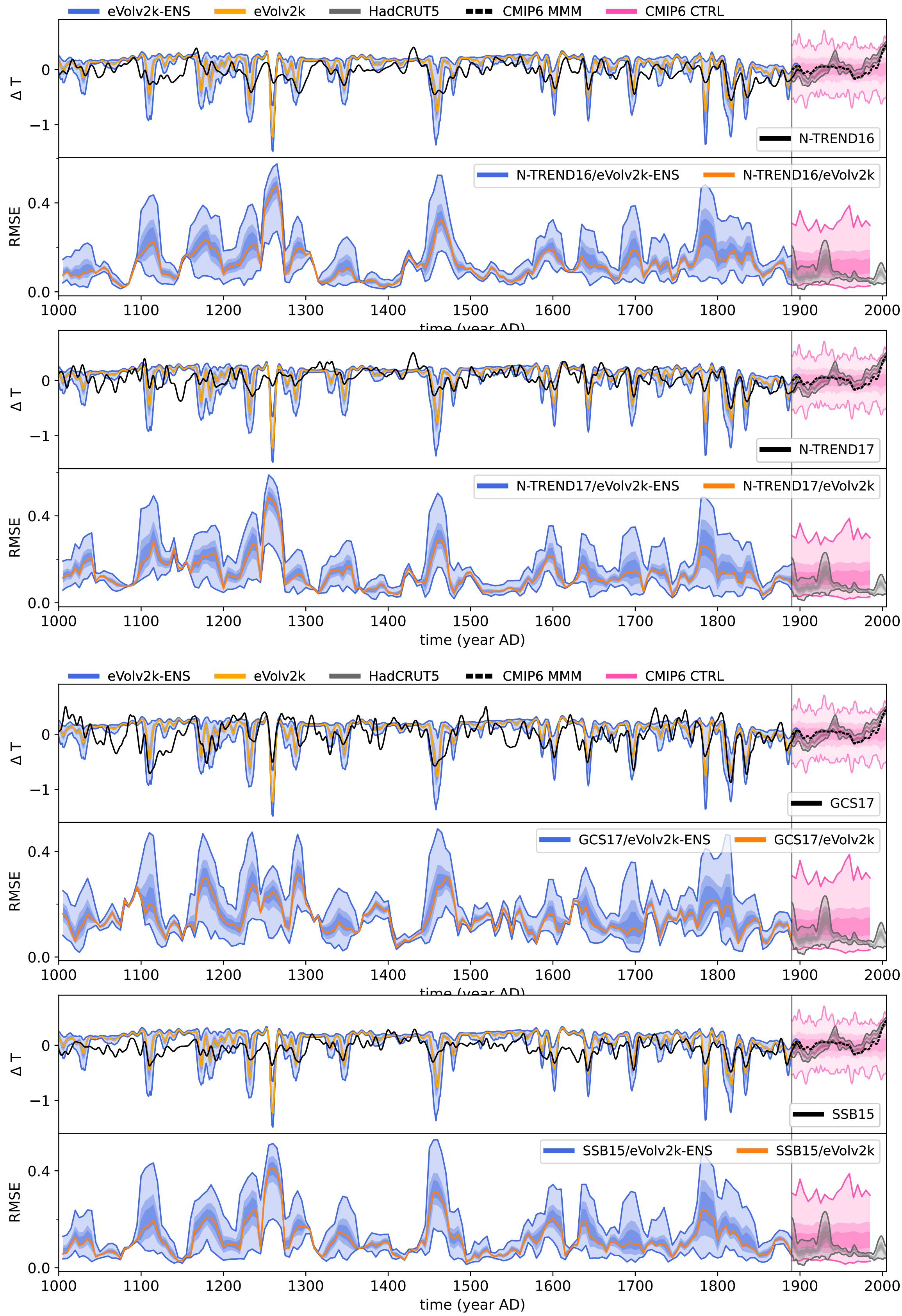


**Figure S21.** As Fig. 4 but for single NH reconstructions. Top to bottom: N-TREND16 (Wilson et al., 2016), N-TREND17 (Anchukaitis et al., 2017), GCS17 (Guillet et al., 2017) and SSB15 (Schneider et al., 2015)

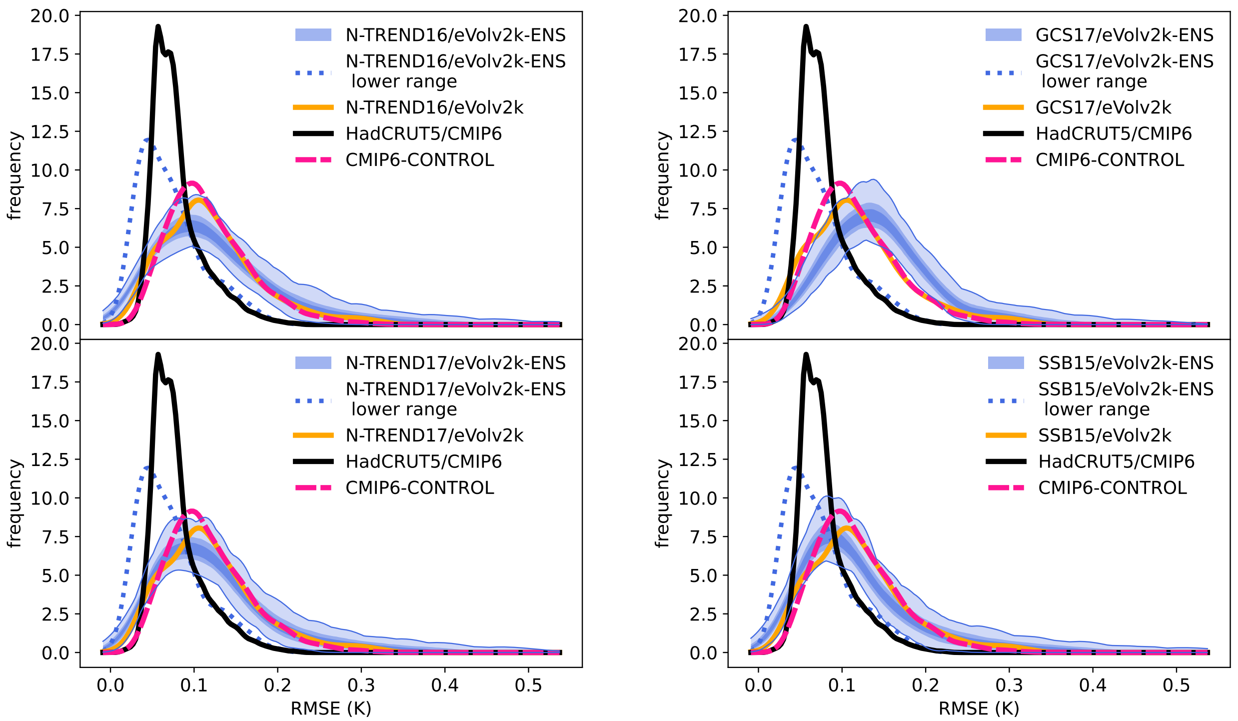


**Figure S22.** As Fig. 5 but for single NH reconstructions. Left top to bottom: N-TREND16 (Wilson et al., 2016), N-TREND17 (Anchukaitis et al., 2017), Right top to bottom: GCS17 (Guillet et al., 2017) and SSB15 (Schneider et al., 2015).

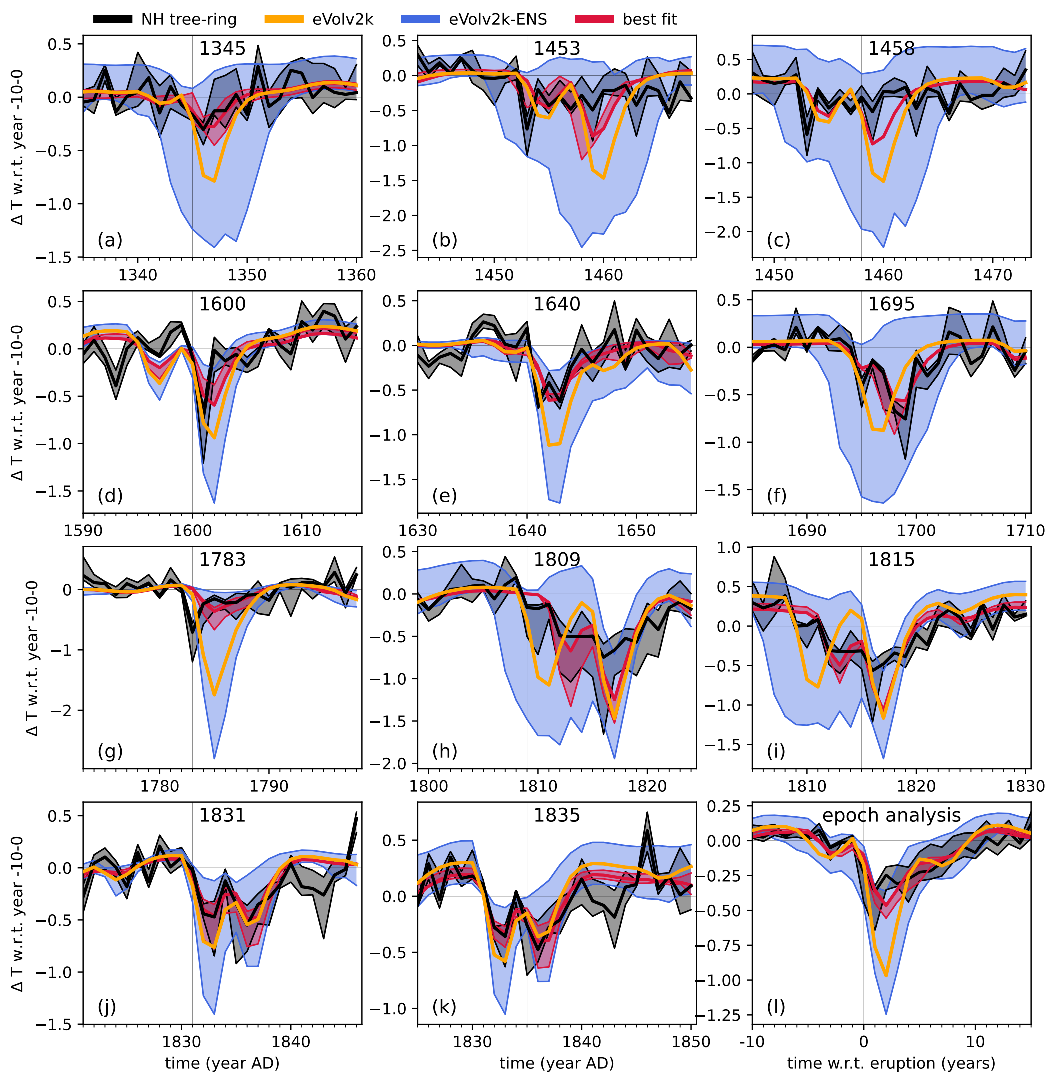


**Figure S23.** As Fig. 6 but for unfiltered data.

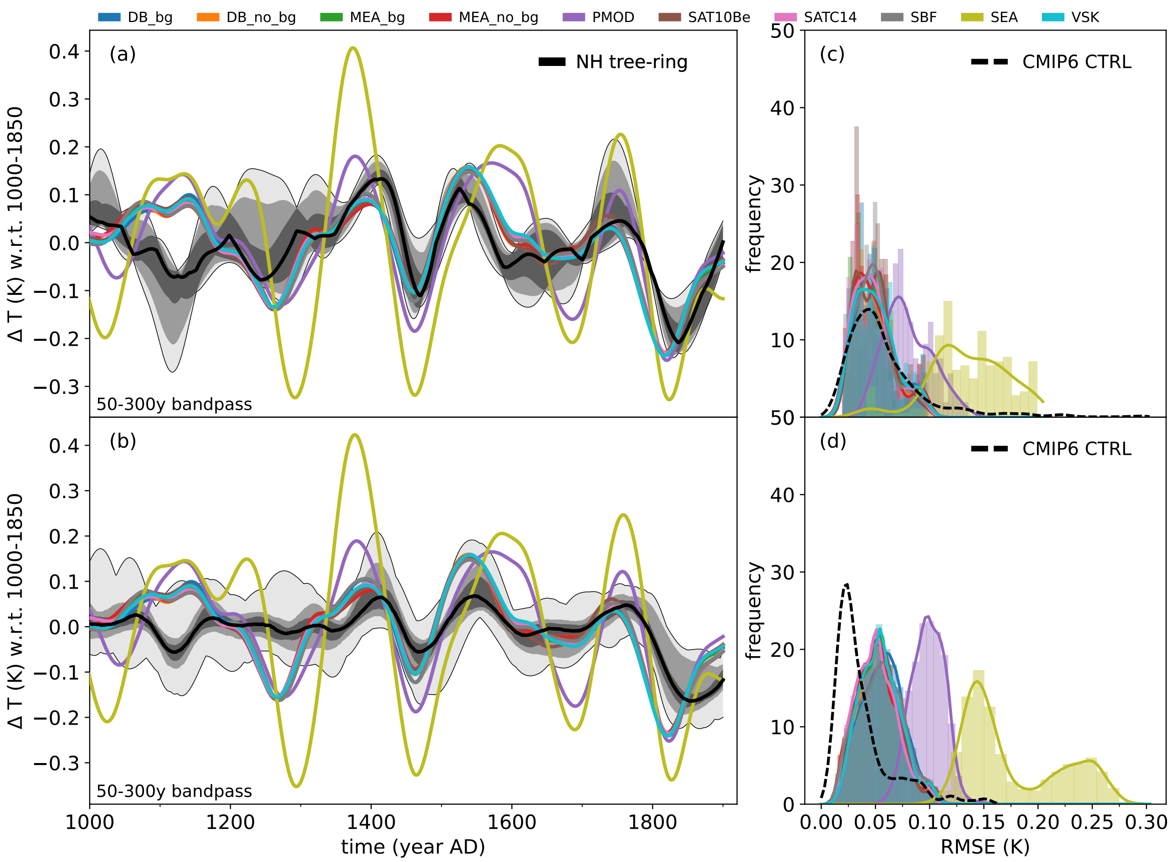


**Figure S24.** As Fig. 3 but for all solar forcings.

| index | Model name | 30y chunks | 170y chunks | runs: specification |
|---|---|---|---|---|
| 1 | ACCESS-CM2 | 16 | 2 | r1i1p1f1 gn |
| 2 | ACCESS-ESM1-5 | 30 | 5 | r1i1p1f1 gn |
| 3 | AWI-CM-1-1-MR | 16 | 2 | r1i1p1f1 gn |
| 4 | AWI-ESM-1-1-LR | 3 | 0 | r1i1p1f1 gn |
| 5 | BCC-CSM2-MR | 20 | 3 | r1i1p1f1 gn |
| 6 | BCC-ESM1 | 15 | 2 | r1i1p1f1 gn |
| 7 | CAMS-CSM1-0 | 16 | 2 | r1i1p1f1 gn |
| 8 | CESM2 | 40 | 7 | r1i1p1f1 gn |
| 9 | CESM2-FV2 | 16 | 2 | r1i1p1f1 gn |
| 10 | CESM2-WACCM | 16 | 2 | r1i1p1f1 gn |
| 11 | CESM2-WACCM-FV2 | 16 | 2 | r1i1p1f1 gn |
| 12 | CNRM-CM6-1 | 16 | 2 | r1i1p1f2 gr |
| 13 | CNRM-CM6-1-HR | 10 | 1 | r1i1p1f2 gr |
| 14 | CNRM-ESM2-1 | 16 | 2 | r1i1p1f2 gr |
| 15 | CanESM5 | 48 | 7 | r1i1p1f1 gn, r1i1p2f1 gn |
| 16 | E3SM-1-0 | 16 | 2 | r1i1p1f1 gr |
| 17 | E3SM-1-1 | 5 | 0 | r1i1p1f1 gr |
| 18 | E3SM-1-1-ECA | 5 | 0 | r1i1p1f1 gr |
| 19 | FGOALS-f3-L | 18 | 3 | r1i1p1f1 gr |
| 20 | FGOALS-g3 | 23 | 4 | r1i1p1f1 gn |
| 21 | FIO-ESM-2-0 | 19 | 3 | r1i1p1f1 gn |
| 22 | GFDL-CM4 | 16 | 2 | r1i1p1f1 gr1 |
| 23 | GFDL-ESM4 | 16 | 2 | r1i1p1f1 gr1 |
| 24 | GISS-E2-1-G | 55 | 7 | r101i1p1f1 gn, r102i1p1f1 gn, r1i1p1f1 gn, r1i1p1f2 gn, r1i1p1f3 gn, r2i1p1f1 gn |
| 25 | GISS-E2-1-G-CC | 5 | 0 | r1i1p1f1 gn |
| 26 | GISS-E2-1-H | 13 | 2 | r1i1p1f1 gn |
| 27 | GISS-E2-2-G | 5 | 0 | r1i1p1f1 gn |
| 28 | HadGEM3-GC31-LL | 16 | 2 | r1i1p1f1 gn |
| 29 | HadGEM3-GC31-MM | 16 | 2 | r1i1p1f1 gn |
| 30 | IITM-ESM | 6 | 1 | r1i1p1f1 gn |
| 31 | INM-CM4-8 | 17 | 3 | r1i1p1f1 gr1 |
| 32 | INM-CM5-0 | 40 | 7 | r1i1p1f1 gr1 |
| 33 | IPSL-CM6A-LR | 74 | 12 | r1i1p1f1 gr, r1i2p1f1 gr |
| 34 | MCM-UA-1-0 | 16 | 2 | r1i1p1f1 gn |
| 35 | MIROC-ES2L | 16 | 2 | r1i1p1f2 gn |
| 36 | MIROC6 | 26 | 4 | r1i1p1f1 gn |
| 37 | MPI-ESM-1-2-HAM | 26 | 4 | r1i1p1f1 gn |
| 38 | MPI-ESM1-2-HR | 16 | 2 | r1i1p1f1 gn |
| 39 | MPI-ESM1-2-LR | 33 | 5 | r1i1p1f1 gn |
| 40 | MRI-ESM2-0 | 23 | 4 | r1i1p1f1 gn |
| 41 | NESM3 | 16 | 2 | r1i1p1f1 gn |
| 42 | NorCPM1 | 48 | 6 | r1i1p1f1 gn, r2i1p1f1 gn, r3i1p1f1 gn |
| 43 | NorESM1-F | 6 | 1 | r1i1p1f1 gn |
| 44 | NorESM2-LM | 16 | 2 | r1i1p1f1 gn |
| 45 | NorESM2-MM | 16 | 2 | r1i1p1f1 gn |
| 46 | SAM0-UNICON | 23 | 4 | r1i1p1f1 gn |
| 47 | TaiESM1 | 16 | 2 | r1i1p1f1 gn |
| 48 | UKESM1-0-LL | 62 | 11 | r1i1p1f2 gn |

**Table S1.** CMIP6 control runs (Eyring et al., 2016)

| event | eVolv2k | eVolv2k–ENS lower | eVolv2k–ENS upper | eVolv2k–ENS best fit of N-TREND16 | N-TREND17 | GCS17 | SSB15 |
|---|---|---|---|---|---|---|---|
| | *VSSI (Tg)* | | | | | | |
| 1345 | 15.1 | 6.4 (42 %) | 24.1 (159 %) | 8.2 (53 %) | 6.7 (44 %) | 6.4 (42 %) | 6.4 (42 %) |
| 1453 | 10.0 | 0.0 (0 %) | 19.5 (195 %) | 17.2 (172 %) | 12.5 (125 %) | 17.2 (172 %) | 12.5 (125 %) |
| 1458 | 33.0 | 16.7 (50 %) | 48.1 (145 %) | 22.6 (68 %) | 16.7 (50 %) | 16.7 (50 %) | 20.6 (62 %) |
| 1600 | 18.9 | 6.2 (32 %) | 34.1 (179 %) | 11.2 (59 %) | 7.6 (40 %) | 11.2 (59 %) | 6.6 (34 %) |
| 1640 | 18.7 | 3.9 (20 %) | 31.3 (167 %) | 11.8 (62 %) | 9.1 (48 %) | 9.5 (50 %) | 9.5 (50 %) |
| 1695 | 15.7 | 6.4 (40 %) | 25.4 (161 %) | 13.5 (86 %) | 13.6 (86 %) | 18.4 (117 %) | 14.7 (93 %) |
| 1783 | 20.8 | 0.0 (0 %) | 43.9 (210 %) | 6.4 (30 %) | 4.5 (21 %) | 13.4 (64 %) | 7.2 (34 %) |
| 1809 | 19.3 | 6.9 (35 %) | 30.8 (159 %) | 13.2 (68 %) | 13.2 (68 %) | 20.3 (105 %) | 12.4 (64 %) |
| 1815 | 28.1 | 15.4 (54 %) | 41.7 (148 %) | 22.6 (80 %) | 22.6 (80 %) | 29.7 (105 %) | 22.0 (78 %) |
| 1831 | 13.0 | 2.3 (17 %) | 22.0 (169 %) | 2.3 (17 %) | 4.9 (38 %) | 9.2 (70 %) | 8.0 (61 %) |
| 1835 | 9.5 | 1.5 (15 %) | 16.7 (176 %) | 10.6 (111 %) | 10.6 (111 %) | 14.8 (156 %) | 4.9 (51 %) |
| | *eruption year* | | | | | | |
| 1345 | 1345 | 1341 (−4) | 1348 (+3) | 1345 (±0) | 1345 (±0) | 1344 (−1) | 1344 (−1) |
| 1453 | 1453 | 1449 (−4) | 1457 (+4) | 1452 (−1) | 1451 (−2) | 1452 (−1) | 1451 (−2) |
| 1458 | 1458 | 1454 (−4) | 1461 (+3) | 1461 (+3) | 1457 (−1) | 1457 (−1) | 1459 (+1) |
| 1695 | 1695 | 1691 (−4) | 1699 (+4) | 1697 (+2) | 1696 (+1) | 1696 (+1) | 1696 (+1) |
| 1809 | 1809 | 1805 (−4) | 1812 (+3) | 1810 (+1) | 1810 (+1) | 1810 (+1) | 1809 (±0) |
| | *eruption month* | | | | | | |
| 1345 | Jan | Jan | Dec | Feb | Sep | Mar | Mar |
| 1453 | Jan | Jan | Dec | Sep | April | Sep | April |
| 1458 | Jan | Jan | Dec | June | Nov | Nov | Mar |
| 1695 | Jan | Jan | Dec | June | June | Feb | Mar |
| 1809 | Jan | Jan | Dec | April | April | July | Mar |

**Table S2.** Eruption specific parameters (VSSI, eruption year, eruption month) for eVolv2k and for the associated best fit eVolv2k–ENS member favoured by the different NH tree-ring reconstructions. Eruption year and month are only shown for the undated eruptions. The relative values compared to eVolv2k are shown in brackets: for VSSI the ratio, for eruption year the difference.

## References

Anchukaitis, K. J., Wilson, R., Briffa, K. R., Büntgen, U., Cook, E. R., D'Arrigo, R., Davi, N., Esper, J., Frank, D., Gunnarson, B. E., Hegerl, G., Helama, S., Klesse, S., Krusic, P. J., Linderholm, H. W., Myglan, V., Osborn, T. J., Zhang, P., Rydval, M., Schneider, L., Schurer, A., Wiles, G., and Zorita, E.: Last millennium Northern Hemisphere summer temperatures from tree rings: Part II, spatially resolved reconstructions, Quaternary Science Reviews, 163, 1–22, https://doi.org/10.1016/j.quascirev.2017.02.020, 2017.

Eyring, V., Bony, S., Meehl, G. A., Senior, C. A., Stevens, B., Stouffer, R. J., and Taylor, K. E.: Overview of the Coupled Model Intercomparison Project Phase 6 (CMIP6) experimental design and organization, Geoscientific Model Development, 9, 1937–1958, https://doi.org/10.5194/gmd-9-1937-2016, 2016.

Guillet, S., Corona, C., Stoffel, M., Khodri, M., Lavigne, F., Ortega, P., Eckert, N., Sielenou, P. D., Daux, V., (Sidorova), O. V. C., Davi, N., Edouard, J.-L., Zhang, Y., Luckman, B. H., Myglan, V. S., Guiot, J., Beniston, M., Masson-Delmotte, V., and Oppenheimer, C.: Climate response to the Samalas volcanic eruption in 1257 revealed by proxy records, Nature Geoscience, 10, 123–128, https://doi.org/10.1038/ngeo2875, 2017.

Nijsse, F. J. M. M., Cox, P. M., and Williamson, M. S.: Emergent constraints on transient climate response (TCR) and equilibrium climate sensitivity (ECS) from historical warming in CMIP5 and CMIP6 models, Earth System Dynamics, 11, 737–750, https://doi.org/10.5194/esd-11-737-2020, 2020.

Parsons, L. A., Brennan, M. K., Wills, R. C., and Proistosescu, C.: Magnitudes and Spatial Patterns of Interdecadal Temperature Variability in CMIP6, Geophysical Research Letters, 47, e2019GL086 588, https://doi.org/10.1029/2019gl086588, 2020.

Schneider, L., Smerdon, J. E., Büntgen, U., Wilson, R. J. S., Myglan, V. S., Kirdyanov, A. V., and Esper, J.: Revising midlatitude summer temperatures back to A.D. 600 based on a wood density network, Geophysical Research Letters, 42, 4556–4562, https://doi.org/10.1002/2015gl063956, 2015.

Wilson, R., Anchukaitis, K., Briffa, K. R., Büntgen, U., Cook, E., D'Arrigo, R., Davi, N., Esper, J., Frank, D., Gunnarson, B., Hegerl, G., Helama, S., Klesse, S., Krusic, P. J., Linderholm, H. W., Myglan, V., Osborn, T. J., Rydval, M., Schneider, L., Schurer, A., Wiles, G., Zhang, P., and Zorita, E.: Last millennium northern hemisphere summer temperatures from tree rings: Part I: The long term context, Quaternary Science Reviews, 134, 1–18, https://doi.org/10.1016/j.quascirev.2015.12.005, 2016.